JOURNAL OF MAGNETIC RESONANCE IMAGING 19:650–656 (2004)

Technical Note

Temperature and SAR Calculations for a Human Head Within Volume and Surface Coils at 64 and 300 MHz

Christopher M. Collins, PhD,[1]* Wanzhan Liu, MS,[1] Jinghua Wang, PhD,[1] Rolf Gruetter, PhD,[2] J. Thomas Vaughan, PhD,[2] Kamil Ugurbil, PhD,[2] and Michael B. Smith, PhD[1]

Purpose: To examine relationships between specific energy absorption rate (SAR) and temperature distributions in the human head during radio frequency energy deposition in MRI.

Materials and Methods: A multi-tissue numerical model of the head was developed that considered thermal conductivity, heat capacity, perfusion, heat of metabolism, electrical properties, and density. Calculations of SAR and the resulting temperature increase were performed for different coils at different frequencies.

Results: Because of tissue-dependant perfusion rates and thermal conduction, there is not a good overall spatial correlation between SAR and temperature increase. When a volume coil is driven to induce a head average SAR level of either 3.0 or 3.2 W/kg, it is unlikely that a significant temperature increase in the brain will occur due to its high rate of perfusion, although limits on SAR in any 1 g of tissue in the head may be exceeded.

Conclusion: Attempts to ensure RF safety in MRI often rely on assumptions about local temperature from local SAR levels. The relationship between local SAR and local temperature is not, however, straightforward. In cases where high SAR levels are required due to pulse sequence demands, calculations of temperature may be preferable to calculations of SAR because of the more direct relationship between temperature and safety.

Key Words: calculations; temperature; MRI; SAR; safety
J. Magn. Reson. Imaging 2004;19:650–656.

TO REDUCE THE RISKS of inducing thermoregulatory imbalance and causing local hyperthermic tissue damage with radio frequency (RF) energy during MRI, the United States' Food and Drug Administration (FDA) and the International Electrotechnical Commission have devised limits on both specific energy absorption rate (SAR) and temperature (T) increases in the human body (1,2). Limits on SAR are given for the average SAR over the whole body, average in the head, and for the maximum volume average over any 1 g (FDA) or 10 g (IEC) region of tissue in the head, body, or extremities (maximum local SAR). It is possible to estimate the average SAR in the head or entire body during an experiment by dividing the time-average input RF power by the mass of the appropriate body section, but determination of the local SAR levels or temperature changes in the human subject is not so easily accomplished. Due to the complicated induced current patterns in the heterogeneous human head, calculations or measurements of the maximum local SAR in simple geometries are not likely to be indicative of the maximum local SAR levels in the head (3). Furthermore, existing limits on the maximum local SAR in any 1 g region of tissue are likely to be exceeded before the limits on average SAR are exceeded (3,4), especially when using local coils, such as surface coils.

When assessing the risk of the RF power in an MR examination, the most important factor is the potential increase in core or local body temperature (1,2). Due to the practical limitations of assessing local temperature increases, however, limits of power deposition are also expressed in SAR limits (1,2). While there are well-studied correlations between T, time, and tissue damage or thermoregulatory distress (5–7), the precise relationship between SAR and temperature is multifactorial. The effect of whole-body SAR on core body temperature is a function of the ability of the body to lose heat by radiation, convection, and evaporation of sweat and is affected by, among other things, body size and type, amount of clothing worn, ventilation, humidity, ambient temperature, and individual response to heat stress. The effect of local SAR on local temperature depends on, among other things, the effects of thermal conduction, perfusion by blood, and the complex heterogeneous geometry of the human body. If the local or core temperature changes enough, there can be local or

[1]Center for NMR Research, Department of Radiology, The Pennsylvania State University College of Medicine, Hershey, Pennsylvania.
[2]Center for MR Research, Department of Radiology, School of Medicine, University of Minnesota, Minneapolis, Minnesota.
Contract grant sponsor: NIH; Contract grant number: R01 EB000454.
Continuation of work presented at ISMRM, Honolulu, 2002. p 704.
*Address reprint requests to: C.M.C., Center for NMR Research, NMR/MRI Building, Department of Radiology H066, The Pennsylvania State University College of Medicine, 500 University Drive, Hershey, PA 17033. E-mail: cmcollins@psu.edu
Received September 5, 2003; Accepted January 29, 2004.
DOI 10.1002/jmri.20041
Published online in Wiley InterScience (www.interscience.wiley.com).

Table 1
Material Properties and Physiological Parameters Used in Calculations

Material/tissue	w (mL/100g/minute)	ρ (kg/m^3)	c (J/kg/°C)	K (W/m/°C)	Q_m (W/m^3)
Air	0	1.3	1006	0.026	0
Blood	1000	1057	3600	0.51	0
Cancellous bone	3	1080	2238	0.36	0
Cerebellum	56	1035.5	3640	0.534	331
Cerebro-spinal fluid	0	1000	4200	0.60	0
Cortical bone	1.4	1850	1300	0.36	0
Esophagus	40	1126	3500	0.527	766
Eye: sclera/cornea	3.8	1151	3000	0.40	0
Eye: vitrous humor	0	1000	4200	0.586	0
Fat	2.8	943	2300	0.23	302
Gray matter	67.1	1035.5	3680	0.565	5370
Mucous membrane,	12	1125	3150	0.343	0
Tendon, other muscle	5.0	10.59	3500	0.498	758
Skin	12	1125	3150	0.343	1125
White matter	23.7	1027.4	3600	0.503	5370

global physiological responses to maintain temperature stability.

The aim of the present study was to simulate the SAR-induced local temperature changes in the human head for three different RF coils. For simplicity, it is assumed that physiological parameters remain independent of temperature. This should be reasonable as long as temperature changes remain small.

MATERIALS AND METHODS

Calculation of SAR

To estimate SAR, full-Maxwell calculations of absorbed power were performed for a human head model in three different coils. The head model was created using the anatomical data from the National Library of Medicine Visible Male Project, using methods described previously (4). The coils that were modeled included a 64 MHz birdcage coil, representative of one type of coil used commonly today, and two specific coils (one surface coil and one volume coil) currently used at 300 MHz. A head model resolution of 2.0 mm in the left-right and anterior–posterior directions and 2.5 mm in the inferior–superior directions was used for calculations with a 64 MHz birdcage coil and 300 MHz quadrature surface coil. A head model resolution of 5.0 mm in each direction was used for calculations with a 300 MHz TEM coil. The geometries and modeling methods for the 64 MHz birdcage coil and the 300 MHz TEM resonator have been described elsewhere (4,8). The methods for modeling the birdcage coil and TEM resonator have been proven accurate by agreement with experiments at frequencies of up to 128 MHz (9) and 300 MHz (8), respectively. The geometry of the quadrature surface coil has been described previously (10). In our study, the quadrature surface coil at 300 MHz was modeled with a method similar to that for the TEM coil (8): first, tuning each coil to 300 MHz (by iteratively adjusting the values of capacitors placed across all gaps in the coil, exciting with a Gaussian impulse, and determining the frequency of the appropriate resonance in a Fourier transformation of the time domain response), then driving the two coils simultaneously with two voltage sources (one in each coil) having a 90° phase difference between them. All electromagnetic field calculations were performed using the finite difference time domain (FDTD) method for electromagnetics (11) using commercially available software (xfdtd; Remcom, State College, PA). The SAR distributions were extracted from the electromagnetic field calculations as described previously (3,4). The maximum local SAR was defined as the average SAR in the 1 cm^3 (FDA) or 10 cm^3 (IEC) volume of tissue having the highest average SAR (3,4). The highest local SAR in the brain was determined by performing the same analysis, but considering only 1 cm^3 or 10 cm^3 regions with a center in white or gray matter.

Calculation of Temperature

Temperature (T) was modeled in the head with a finite difference implementation of the Pennes bioheat equation (12):

$$\rho c \frac{dT}{dt} = \nabla \cdot (k\nabla T) + [-\rho_{blood} w c_{blood}(T - T_{core})] + Q_m + SAR\rho \quad (1)$$

where the different values for ρ (material density), c (heat capacity), k (thermal conductivity), w (perfusion by blood), and Q_m (heat generated by metabolism) for several different tissues were acquired from the literature (13–17). The values used in these calculations are given in Table 1, unless otherwise specified. The finite difference implementation was achieved by using first order central difference approximations for all derivatives with respect to position and a first order forward difference approximation for the derivative with respect to time. Solving for T at a time in the future by one time increment Δt yields the algebraic equation:

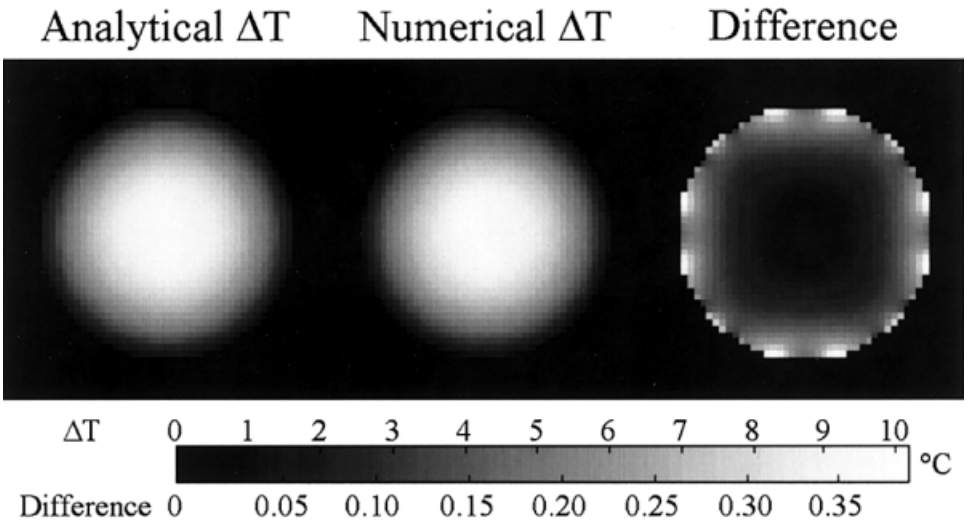

Figure 1. Analytically (left) and numerically (center) calculated increase in temperature (ΔT) distributions for the sphere of unperfused brain tissue after application of uniform SAR of 3.0 W/kg, and the difference (right) of the numerically calculated value from the analytically calculated value. Grayscale values are given in °C.

$$T_{\tau+1} = T + \frac{\Delta t}{\rho c}\left\{\frac{(K_{i+1}T_{i+1} - K_{i+1}T_{i-1} - K_{i-1}T_{i+1} + K_{i-1}T_{i-1}) \div 4 + K(T_{i+1} - 2T + T_{i-1})}{(\Delta x)^2} + \frac{(K_{j+1}T_{j+1} - K_{j+1}T_{j-1} - K_{j-1}T_{j+1} + K_{j-1}T_{j-1}) \div 4 + K(T_{j+1} - 2T + T_{j-1})}{(\Delta y)^2} + \frac{(K_{k+1}T_{k+1} - K_{k+1}T_{k-1} - K_{k-1}T_{k+1} + K_{k-1}T_{k-1}) \div 4 + K(T_{k+1} - 2T + T_{k-1})}{(\Delta z)^2} + SAR\rho - \frac{wc_{blood}\rho_{blood}(T - T_{blood})}{6000} + Q_m\right\} \quad (2)$$

where the indices i, j, and k indicate spatial location in the x, y, and z directions, respectively, and the index τ indicates position in time. Increments in space are Δx, Δy, and Δz, and the size of the time step is Δt. Subscripts for K and T indicate only deviation from the location (i, j, k) and the time τ. The factor of 6000 in the denominator of the perfusion term is necessary to achieve dimensional equivalence with all other terms in the equation (18) by converting the units for w from mL/100 g/minute to mL/g/second. The temperature of all air outside of the head was held constant at 23°C.

In general, the temperature distribution for a given set of parameters, including an SAR distribution, was calculated by starting with an initial condition (IC), or initial guess, for temperature at each location, then iteratively solving for the correct temperature distribution by solving for T at future points in time with Eq. [2]. The exact value of the initial condition did not affect the final calculated temperature distribution, but could affect the number of iterations required to reach this final calculated distribution. If the temperature distribution is given or known at time τ for a given location (i, j, k), Eq. [2] has only one unknown, namely the temperature at the next point in time, $T_{\tau+1}$. Thus, an algebraic equation is solved at each location at progressive points in time for the temperature at the next point in time until a new equilibrium is reached where the temperature no longer changes with time. Using this method, we modelled a situation where a given SAR distribution is applied until the maximum temperature increase results.

Validation of Temperature Calculation Method

Verification of our finite difference implementation was performed by comparison to two analytical solutions. The first comparison was to an analytical solution for equilibrium temperature distribution in an unperfused sphere of brain tissue with a uniform SAR of 3.0 W/kg (19). For this calculation, the sphere had a diameter of 40 cells with a cell resolution of 5 mm in each dimension and material properties equal to the average of those for gray and white matter as shown in Table 1. In the second comparison, numerical results were compared to an analytical solution for a perfused sphere of tissue with no thermal conductivity and with a uniform SAR of 3.0 W/kg (18). In this case, we employed the same tissue parameters as used by Athey (18), most significantly ρ_{blood} = 1040 kg/m^3, w = 10 mL/100 g/minute, and c_{blood} = 4026 J/kg/°C. The initial condition for both of these calculations was that all temperatures were equal to that of ambient air (23°C) and the temperature of blood was constant at 37°C.

Calculations for the Human Head in MRI

Calculations of equilibrium temperature distributions for the human head in three different coils at two different frequencies were performed. It was assumed that rates of perfusion were independent of time and temperature and that the temperature of blood was constant at 37°C. An initial equilibrium temperature distribution was first calculated and recorded with SAR = 0 W/kg and IC of all tissue temperatures equal to core body temperature. Then, RF fields were normalized so as to induce a head-average SAR of either 3.0 W/kg, the current nonsignificant risk FDA limit (2), or 3.2 W/kg, the current IEC normal mode limit over any 6 minute period (1), were applied to the model. When it reached a new equilibrium, the temperature distribution was recorded.

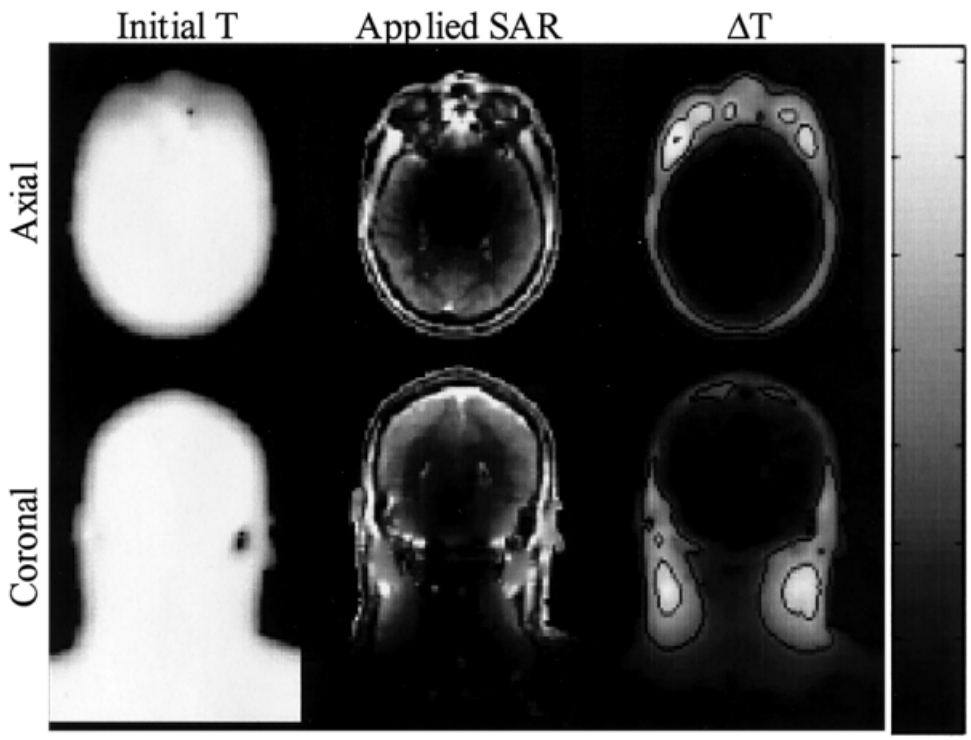

Figure 2. Initial equilibrium temperature distribution (left), applied SAR distribution for 64 MHz birdcage coil (center), and resulting increase in temperature (ΔT) at new equilibrium (right) on axial (top) and coronal (bottom) slices through the head. Linear grayscale is from 23 (black) to 37°C (white) for initial temperature, 0 to 10 W/kg for applied SAR, and 0 to 1.5°C for resulting temperature increase. Contours in plots of ΔT placed at 0.5, 1.0, and 1.5°C. The black regions in the initial temperature distribution plots (left) are due to air-filled sinuses.

RESULTS

The numerically calculated increase in temperature (ΔT) after application of a uniform SAR of 3.0 W/kg to a 20 cm diameter sphere of unperfused brain tissue was compared to an analytical solution of the same problem in Fig. 1. The largest difference between these two calculations is about 0.387°C, occurring at the surface of the model where the discretized nature of the numerical model makes it impossible to match the smooth, spherical surface in the analytical calculations.

For the calculation of the perfused sphere with uniform SAR and no thermal conductivity, the temperature of the sphere was 37.588°C in the numerical solution, as compared to 37.573°C in the analytical solution—an inconsequential difference of 0.015°C.

Figure 2 shows the equilibrium temperature distribution in the head before the RF field is applied, the SAR distribution during coil excitation for an average SAR of 3.2 W/kg in the head in a birdcage coil at 64 MHz, and the resulting temperature increase (ΔT) at the new equilibrium. There is a gradient in the initial temperature distribution from about 37.3°C at the center of the brain to about 32°C at the skin. The spatial distribution of SAR and increase in temperature for the head in the TEM at 300 MHz (not shown) are very similar to those in Fig. 2, but slightly less symmetric. The SAR distribution is also slightly less concentrated toward the periphery of the head at 300 MHz, as is consistent with previous calculations of SAR distribution as a function of frequency (4). In these calculations, the temperature increases are greatest in tissues that are not well perfused, such as muscle at rest and the eye.

Figure 3 shows the distribution of the circularly-polarized component of the RF magnetic field that rotates

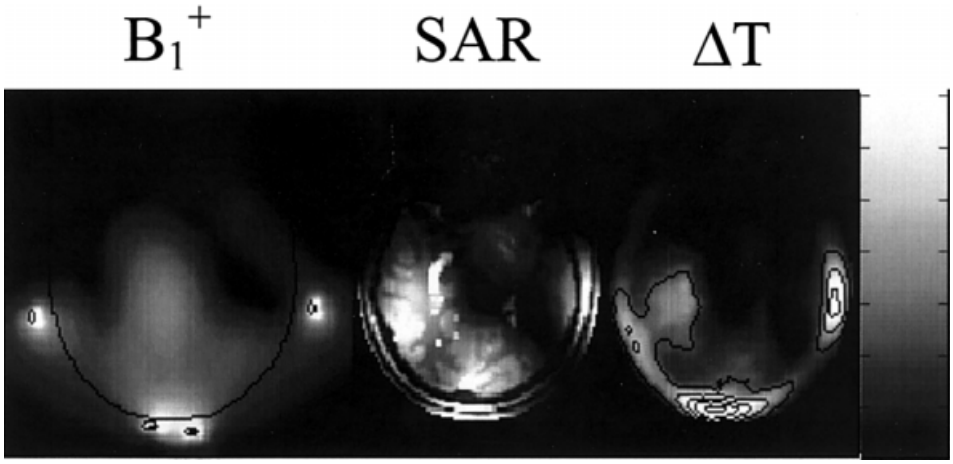

Figure 3. Distributions of B_1^+ (left), SAR (center), and resulting temperature increase (right) for quadrature surface coil at 300 MHz. Linear grayscale is from 0 (black) to 15 mT (white) for B_1^+, 0 to 20 W/kg for SAR, and 0 to 1.5°C for temperature increase. Contours for temperature increase at 0.5, 1, 1.5, 2.0, and 2.5°C.

Table 2
Maximum SAR in Any 1 cm^3 Region for Head Average SAR of 3.0 W/kg for Comparison to FDA Limits

RF coil	Maximum local SAR in head		Maximum local SAR in brain only	
	Location	Value (W/kg)	Location	Value (W/kg)
Birdcage coil at 64 MHz	Skin and facial muscle inferior to eye	16.2	Superior cerebrum, partially including SSS	13.7
TEM coil at 300 MHz	Muscle tissue in masticator space	16.1	Superior cerebrum, partially including SSS	11.8
Surface coil at 300 MHz	Superior sagittal sinus	53.8	Mid-posterior cerebrum, partially including SSS	50.7

SSS = superior sagittal sinus.

in the same direction as nuclear precession (B_1^+), the SAR distribution, and the resulting temperature increase for the quadrature surface coil at 300 MHz. Although the SAR distribution appears to be asymmetric, the B_1^+ distribution is more symmetric and is consistent with that required to produce symmetric images of the brain at 300 MHz (10).

For comparison to FDA limits, the location and value of the maximum SAR in any 1 g of tissue in the head and in the brain are given in Table 2. For the cases where each coil is driven to induce 3.0 W/kg average SAR over the head, the location and maximum ΔT in the head and in the brain are given in Table 3. Similarly, for comparison to IEC limits, the location and value of the maximum SAR in any 10 g region of tissue in the head and in the brain are given in Table 4. For the cases where each coil is driven to induce 3.2 W/kg average SAR over the head, the location and maximum ΔT in the head and in the brain are given in Table 5.

DISCUSSION

Temperature distributions calculated with the methods presented here are in good agreement with analytically-calculated temperatures for simple objects and simple SAR distributions. The agreement between numerically and analytically calculated temperature in an unperfused sphere with uniform SAR (Fig. 1) would be improved further with a higher resolution grid or by higher order finite difference approximations, but both of these options would require a significant increase in calculation time. The resolution and sphere size presented are similar to the resolutions and head size used in this study. In the presence of the moderating effects of perfusion, the difference between numerical simulation and reality should be significantly less than the difference shown in Fig. 1, as all ΔT would be significantly less than those calculated here with no perfusion. Numerically-calculated temperature in a perfused sphere with no thermal conductivity is in nearly perfect agreement with analytical calculations for the same case. Unfortunately, there was no analytical solution found for a three-dimensional geometry that considered both perfusion and thermal conduction.

In the normal human body, thermoregulatory mechanisms act to oppose local and global temperature changes. Assuming a head mass of about 5 kg and a body mass of about 60 kg, an average SAR of 3.2 W/kg in the head would result in a whole-body average SAR of about 0.27 W/kg. This is well below an SAR expected to affect the core body temperature or cause any systemic thermoregulatory effects (e.g., increased respiratory rate, whole-body cutaneous vasodilation coupled with increased heart rate and decreased blood pressure, or whole-body sweating) (1). In normal tissues, vasodilation resulting in increased perfusion, as well as local sweating in the skin, can occur locally in response to local increases in temperature. Though the relationship between local perfusion rates and local temperatures is not well established for many tissues, there is no significant increase in the local perfusion rate in muscle tissue until a temperature increase of about 4°C is induced (20). Similarly, when core body temperature is 37°C, local sweating in skin does not occur until the local skin temperature increases above its initial temperature by a few degrees (21). Neither of these conditions are met in the calculations presented here, except in the case of the quadrature surface coil driven to induce a 3.0 or 3.2 W/kg SAR averaged over the head. As discussed later in this study, this is an extremely large amount of power for this coil. Therefore, for volume head coils driven at power levels up to the regula-

Table 3
Maximum Temperature Increase (ΔT) for Head Average SAR of 3.0 W/kg for Comparison to FDA Limits

RF coil	Maximum ΔT in whole head		Maximum ΔT in brain only	
	Location	Value (°C)	Location	Value (°C)
Birdcage coil at 64 MHz	Muscle tissue in masticator space	2.1	Frontal lobe at anterior and inferior surface	0.9
TEM coil at 300 MHz	Muscle tissue in masticator space	2.4	Gray matter nearest masticator space	0.7
Surface coil at 300 MHz	Scalp behind cerebellum	4.3	Posterior cerebellum	1.7

Table 4
Maximum SAR in Any 10 cm^3 Region for Head Average SAR of 3.2 W/kg for Comparison to IEC Limits

RF coil	Maximum local SAR in head		Maximum local SAR in brain only	
	Location	Value (W/kg)	Location	Value (W/kg)
Birdcage coil at 64 MHz	Muscle tissue in masticator space	10.7	Superior cerebrum, partially including SSS	8.92
TEM coil at 300 MHz	Superior cerebrum, partially including SSS	8.73	Superior cerebrum, partially including SSS	8.73
Surface coil at 300 MHz	Mid-posterior cerebrum, partially including SSS	28.7	Mid-posterior cerebrum, partially including SSS	28.7

SSS = superior sagittal sinus.

tory limits on head-average SAR, it may be reasonable to neglect the physiological response to temperature, as was done in this study. For other cases, including the case of the quadrature surface coil driven to induce a 3.0 or 3.2 W/kg SAR averaged over the head, results of the methods used here would indicate a temperature change larger than expected in the presence of a functioning thermoregulatory system.

In all calculations considering the head, we assumed perfusion rates comparable to those in the healthy human. It is important to note that temperature increases might be higher in patients with impaired cerebral perfusion, such as those with a stroke, tumor, or arteriovenous malformations. The present head model was based on an anatomy typical for relatively young adults and for tissue properties from the literature. The results may vary with age as the geometry, composition, and material properties of human tissues change (22), and will also vary between individuals. The flow of CSF was not taken into account in the present simulation.

In agreement with previous publications (3,4), the results in Table 2 indicate that the nonsignificant risk FDA limit on SAR in any 1 g region in the head (8 W/kg) will be exceeded before the nonsignificant risk FDA limit on head-average SAR (3 W/kg) is exceeded for both volume and surface coils intended for head imaging. Similarly, the results in Table 4 indicate that the normal mode IEC limit on SAR in any 10 g region in the head (10 W/kg) will be exceeded before the normal mode IEC limit on head-average SAR (3.2 W/kg) is exceeded, except in the TEM coil at 300 MHz.

The results in Tables 3 and 5 indicate that when a volume coil is driven to produce 3.2 W/kg average SAR in the head, it is unlikely that any increase in T much above 1°C (IEC normal mode limit for increase in temperature anywhere in the head) will occur in brain tissue, whether at 64 or at 300 MHz. Our calculations indicate that T may increase by more than 1°C within the head but outside of the brain. Because local heating in some regions of the brain (especially in the hypothalamus) may result in confusion of the whole-body thermoregulatory system (23), it is important to ensure that no significant temperature increase occurs in the brain. But, just as tissues in the extremities are expected to withstand local ΔT of up to 3°C (1), tissues in the head, other than the brain (e.g., skin, muscle, fat, bone, and tissues in the eye) (6,24), should be able to withstand ΔT of up to a few °C with no irreversible effects. For this reason, we present both maximum ΔT in the entire head and in the brain only, though the IEC guidelines place the limit for ΔT at 1°C anywhere in the head.

When the quadrature surface coil is driven to induce 3.2 W/kg SAR averaged over the entire the head, the maximum ΔT within the brain tissue is 1.85°C, well above the 1°C limit. In agreement with the IEC guidelines (1), this indicates that when using transmit surface coils, whole-head SAR limits are not a good guide and extra caution should be exercised. Because they are exciting much smaller volumes, however, surface coils generally require much less power than do volume coils. For example, proton decoupling can be accomplished with the quadrature surface coil, modeled here, with only 4 W of power and a 2.4% duty cycle (unpublished experimental results). But even with 4 W of power and a 100% duty cycle (about 0.55 W/kg averaged over the head), the maximum ΔT within the brain is only 0.32°C, the maximum ΔT in the head is 0.785°C, and the maximum SAR in any 1 g of tissue in the head is 9.90 W/kg, as was calculated using the numerical methods presented here.

The highest local SAR in the brain is consistently found adjacent the superior sagittal sinus. This is be-

Table 5
Maximum Temperature Increase (ΔT) for Head Average SAR of 3.2 W/kg for Comparison to IEC Limits

RF coil	Maximum ΔT in whole head		Maximum ΔT in brain only	
	Location	Value (°C)	Location	Value (°C)
Birdcage coil at 64 MHz	Muscle tissue in masticator space	2.2	Frontal lobe at anterior and inferior surface	0.9
TEM coil at 300 MHz	Muscle tissue in masticator space	2.6	Gray matter nearest masticator space	0.7
Surface coil at 300 MHz	Scalp behind cerebellum	4.5	Posterior cerebellum	1.8

cause the method used for finding the highest local SAR in the brain consisted of averaging SAR over volumes with a center in the brain, but which could potentially have peripheral regions in other tissues. Because of the geometry and location of the superior sagittal sinus and due to the relatively high conductivities of the materials it contains (especially blood), SAR levels in the superior sagittal sinus are typically very high compared to those in the brain, although ΔT in the superior sagittal sinus is typically very low due to the high rate of blood flow.

There is not good spatial correlation between SAR and temperature increase, the physiologically relevant parameter in evaluating risk. This is a result of the complex, multifactorial relationship between temperature and SAR. In areas with high perfusion, such as the brain, moderate to high SAR levels can result in minimal temperature increase, while in areas with lower perfusion, such as muscle at rest and the eye, temperature may increase even with relatively low SAR levels (Fig. 2). It is also apparent from Fig. 3 that thermal energy can be transferred to bone from surrounding tissues by thermal conduction. This relatively efficient conductive heat transfer to bone is consistent with expectations from work in hyperthermia (25). Due to the combined effects of perfusion and thermal conduction in the heterogeneous human head, the location of maximum local SAR corresponds to that of maximum temperature increase in very few of the cases evaluated in this study (Tables 2–5).

It is noteworthy that in all of the situations presented here, FDA limits on SAR in any 1 g region in the head and IEC limits on SAR in any 10 g region in the head would be exceeded before the temperature in the brain increased by more than 1°C. Due to the relative difficulty of predicting temperature in the human head, safety limits based on estimates of local SAR levels may be the simpler and more conservative approach, although less relevant in terms of risk.

REFERENCES

1. International Electrotechnical Commission. International standard, medical equipment–part 2: particular requirements for the safety of magnetic resonance equipment for medical diagnosis, 2nd revision. Geneva: International Electrotechnical Commission 601-2-33; 2002. pp 29–31.
2. Center for Devices and Radiologic Health. Guidance for the submission of premarket notifications for magnetic resonance diagnostic devices. Rockville: Food and Drug Administration; 1998. p 21.
3. Collins CM, Li S, Smith MB. SAR and B1 field distributions in a heterogeneous human head model within a birdcage coil. Magn Reson Med 1998;40:847–856.
4. Collins CM, Smith MB. Signal-to-noise ratio and absorbed power as functions of main magnetic field strength and definition of "90°" RF pulse for the head in the birdcage coil. Magn Reson Med 2001;45: 684–691.
5. Moritz AR, Henriques FC. Studies of themal injury II. The relative importance of time and surface temperature in the causation of skin burns. Am J Pathol 1947;23:695–720.
6. Guy AW, Lin JC, Kramar PO, Emery AF. Effect of 2450-MHz radiation on the rabbit eye. IEEE Trans Microwave Theory Tech 1975; 23:492–498.
7. Shellock FG, Schaeffer DJ, Crues JV. Alterations in body and skin temperatures caused by magnetic resonance imaging: is the recommended exposure for radiofrequency radiation too conservative? Br J Radiol 1989;62:904–909.
8. Vaughan JT, Garwood M, Collins CM, et al. 7T vs. 4T: RF power, homogeneity, and signal-to-noise comparison in head images. Magn Reson Med 2001;46:24–30.
9. Alecci M, Collins CM, Smith MB, Jezzard P. Radio frequency magnetic field mapping of a 3 Tesla birdcage coil: experimental and theoretical dependence on sample properties. Magn Reson Med 2001;46:379–385.
10. Wang JH, Yang QX, Collins CM, et al. The polarization of the radio frequency field in a human head at high field: a study with a quadrature surface coil at 7.0 Tesla. Magn Reson Med 2002;48: 362–369.
11. Yee KS. Numerical solution of initial boundary value problems involving Maxwell's equations in isotropic media. IEEE Trans Antennas Propagat 1966;14:302–307.
12. Pennes HH. Analysis of tissue and arterial blood temperatures in the resting human forearm. J Appl Physiol 1948;1:93–122.
13. Duck FA. Physical properties of tissue, a comprehensive reference book. London: Academic Press; 1990. p 13–28, 138–140, 329.
14. Schreiber WG, Guckel F, Stritzke P, Schmiedek P, Schwartz A, Brix G. Cerebral blood flow and cerebrovascular reserve capacity: estimation by dynamic magnetic resonance imaging. J Cereb Blood Flow Metab 1998;18:1143–1156.
15. Tropea BI, Lee RC. Thermal injury kinetics in electrical trauma. J Biomech Eng 1992;114:241–250.
16. Hand JW, Lau RW, Lagendijk JJW, Ling J, Burl M, Young IR. Electromagnetic and thermal modeling of SAR and temperature fields in tissue due to an RF decoupling coil. J Magn Reson Imaging 1999;42:183–192.
17. van Leeuwen GMJ, Hand JW, Lagendijk JJW, Azzopardi DV, Edawards AD. Numerical modelling of temperature distributions within the neonatal head. Pediatr Res 2000;48:351–356.
18. Athey TW. A model of temperature rise in the head due to magnetic resonance imaging procedures. Magn Reson Med 1989;9:177–184.
19. Reynolds WC, Perkins HC. Engineering thermodynamics. New York: McGraw-Hill; 1977. p 549.
20. Sekins KM, Lehmann JF, Esselman P, et al. Local muscle blood flow and temperature responses to 915MHz diathermy as simultaneously measured and numerically predicted. Arch Phys Med Rehabil 1984;65:1–7.
21. Nadel ER, Mitchell JW, Saltin B, Stolwijk JAJ. Peripheral modifications to the central drive for sweating. J Appl Physiol 1971;31: 828–832.
22. Dobbing J, Sands J. Quantitative growth and development of the human brain. Arch Dis Child 1973;48:757–767.
23. Precht H, Christopherson J, Hensel H, Larcher W. Temperature and life. New York: Springer-Verlag; 1973. p 567–571.
24. Mainster MA, Khan JE. Photic retinal injury. In: Ryan S, editor. Retina. St. Louis: Mosby; 1994. p 1767–1781.
25. Hahn GM. Hyperthermia for the engineer: a short biological primer. IEEE Trans Biomed Eng 1984;31:3–8.